On the measurement and analysis of data from transient heat transfer experiments

GeonHwan Cho, Hui Tang, J. Michael Owen, Gary D Lock*

Department of Mechanical Engineering
University of Bath
Bath, BA2 7AY, UK

*Corresponding author: Gary D. Lock
Tel: +44(0)1225 38 6854
e-mail: ensgdl@bath.ac.uk

Keywords: MLE, transient heat transfer, infra-red, Fourier's equation

Abstract

This paper describes a new method to determine the heat transfer coefficient, h, and the adiabatic-surface temperature, T_{ad}, from transient measurements of the surface temperature of a test piece. Maximum Likelihood Estimation (MLE) is used in conjunction with Fourier's 1D equation to determine the optimum values of h and T_{ad}, and also their 95% confidence intervals, without having to measure the air temperature. Validation experiments are conducted in a small purpose-built wind tunnel, and a novel infra-red (IR) sensor is used to measure the surface temperature of the test piece. A mesh heater is used to generate either a step-change in the air temperature or a 'slow-transient' in which the air temperature - and consequently T_{ad} – increases slowly with time. Numerical simulations, using 'noisy data', show that the computations give accurate estimates of h and T_{ad} for both the step-change and slow-transient cases. The values of h and T_{ad} determined from the measurements in the wind-tunnel are in good agreement with empirical correlations for turbulent flow over a flat plate.

An advantage of the new method is that it can be used for all transient experiments, even those slow transients that violate the assumption of a semi-infinite solid, an assumption that is used in most existing analysis methods. The new method, which was applied here to boundary-layer flow with one stream of fluid, could also be applied to 'three-temperature problems', like film cooling, which involve two streams of fluid. The significant advantage of using the method for these problems is that *both* h and T_{ad} could be determined accurately from a *single* experiment.

Nomenclature

A	cross-sectional area of wind-tunnel
A_e	effective area of the freestream outside boundary layer (δ^*)
Bi	Biot number ($= hL/k_s$)
C	constants
C_p	specific heat
Fo	Fourier number ($= \alpha t/L^2$)
Fo_τ	nondimensional time constant ($= \alpha\tau/L^2$)
g	gravitational acceleration
Gr	Grashof number
h	heat transfer coefficient
k	thermal conductivity
l	vertical height of IR sensor; negative log of likelihood function
L	thickness of solid
N	number of data points
$\mathcal{N}$	normal distribution
Nu	Nusselt number($= hx/k_{air}$)
P	likelihood function
Pr	Prandtl number
q_s	heat flux from fluid to solid
R	recovery factor

Re	Reynolds number$(= \rho U x/\mu)$
T	temperature
t	time
u	streamwise velocity inside boundary layer
U_0	freestream velocity at $x = 0$
U_∞	velocity of the free stream outside boundary layer
x	streamwise coordinate measured from mesh heater
y	normal distance from surface in boundary layer
Z	nondimensional value of z $(= z/L)$
z	normal distance from surface in solid
α	thermal diffusivity $(= k/\rho C_p)$
β	volume expansion coefficient
β_n	eigenvalue in quenching solution
δ	boundary layer thickness
δ^*	displacement thickness
Θ	theoretical nondimensionial temperature$(= (T - T_{in})/(T_{ad} - T_{in}))$
θ	experimental nondimensionial temperature$(= (T - T_{in})/(T_{s,max} - T_{in}))$
μ	dynamic viscosity
ν	kinematic viscosity
ρ	density
σ	standard deviation
τ	time constant
ϕ	parameters in MLE
χ	parameter in semi-infinite solution $\left(= BiFo^{1/2}\right)$

Subscripts

ad	adiabatic
air	air
amb	ambient
f	film
in	initial value
IR	infra-red
L	back face of solid
max	maximum
o	parameters estimated from MLE
ref	appropriate reference value
s	experimental value on surface; surface
$turb$	turbulent
w	true value on surface
x	value at distance x from mesh
τ	time constant
∞	freestream value

Acronyms

CI	confidence interval
IR	infra-red
MLE	maximum likelihood estimation
PID	proportional integral derivative

1. Introduction

The object of most heat transfer experiments is to determine the heat transfer coefficient, h, which is defined here as

$$h = \frac{q_s}{(T_{ad} - T_s)} \qquad (1.1)$$

where, q_s is the convective heat flux from a fluid into the solid, and T_s and T_{ad} are the surface and adiabatic temperatures respectively. This definition ensures that, for a finite value of h, $q_s = 0$ when $T_s = T_{ad}$. In general, T_{ad} depends on the fluid dynamics, and for external boundary-layer flows it can often be calculated from

$$T_{\mathrm{ad}} = T_\infty + R\frac{U_\infty^2}{2C_p} \qquad (1.2)$$

where, T_∞ and U_∞ are the static temperature and velocity of the free stream outside the boundary layer, C_p is the specific heat of the fluid and R is the recovery factor, which depends on the Prandtl number of the fluid and on whether the flow is laminar or turbulent. For many practical cases, T_{ad} is unknown.

The development of thermochromic liquid crystal (TLC) in the 1980s makes it relatively simple, providing there is suitable optical access, to measure the variation of T_s with time over the entire surface of a solid test piece. The test piece is usually made from a material that is a poor thermal conductor (e.g. acrylic or polycarbonate, where $k \approx 0.2\mathrm{W/mK}$), and the values of h and T_{ad} can then be determined from the inverse solution of the one-dimensional (1D) Fourier's equation. (The term *inverse solution* refers to the case where h is determined from the known variation of T_s with time; the *direct solution* refers to the case where the variation of T_s with time is calculated from a known value of h.)

A narrow-band crystal can be used to determine the time at which the surface of a test piece reaches the activation temperature of the crystal. If T_{ad} is known and if a step-change in T_∞ can be generated (by a mesh heater, for example), h can be calculated from analytical solutions of the 1D Fourier's equation for a semi-infinite solid. This method of determining h has been discussed by, for example, Jones and Hippensteele (1988), Kasagi *et al.* (1989), Camci *et al.* (1991) and Baughn (1995).

In a similar manner, two narrow-band crystals can be used to calculate both T_{ad} and h. Treuren *et al.* (1994), Pountney *et al.* (2013) evaluated both h and T_{ad} in this way by using a coating of several narrow-band crystals. However, as shown by Yan and Owen (2002), judicious choice of crystal is needed to minimise the uncertainties in h and T_{ad}, and the uncertainty in the computed h will be larger than that for the case where T_{ad} is known. In addition, these methods are only applicable for transient experiments with a step-change in T_∞, which is not always possible.

Even if a step-change can be generated by the upstream heater, the transient temperature of the fluid at the test section is unlikely to remain constant, and it can be seen from Eq. (1.2) that if T_∞ varies with time then T_{ad} must also vary with time. For these so-called *slow-transient cases*, the measured surface-temperature history can be used as a boundary condition for the solution of Fourier's equation for a semi-infinite solid to determine both h and T_{ad}. For the case where the air temperature rises exponentially with time, Gillespie *et al.* (1998) obtained an analytical solution of Fourier's equation, which was then used to determine h from transient experiments. Newton *et al.* (2003) further developed the technique using two crystals to determine h and T_{ad} by representing the measured temperature rise of the air by an exponential series; the series was then used as a boundary condition for Fourier's equation. Kan *et al.* (2014) evaluated h and T_{ad} by applying Duhammel's theorem to time-varying temperatures measured at several locations inside a finned channel.

In all the above slow-transient cases, Fourier's equation was solved for a *semi-infinite solid*, which – as discussed in Section 2.1 below – limits the time for which the solution is valid. In some cases – like those discussed by Pountney et al. (2013) – the long time-constant for the air temperature can violate the semi-infinite assumption. In such cases, the boundary conditions on *both surfaces* of the test piece have to be used in the inverse solution of Fourier's equation. However, inverse solutions are error-prone: small errors in the measured values of T_s can create very large uncertainties in the computed values of h and T_{ad}. In this paper, it is shown how the statistical technique of Maximum Likelihood Estimation (MLE) can be used to accurately determine both h and T_{ad}, and their confidence intervals, from the numerical solution of Fourier's equation. The method is applicable to all cases, even those slow transients that violate the semi-infinite-solid assumption.

In principle, the MLE method could also be applied to the so-called *three-temperature problem* for film-cooled surfaces, where the heat transfer depends not only on T_s and T_∞ but also on the film temperature, T_f. For these cases, T_{ad}, which depends on both T_∞ and T_f, is often determined from steady-state experiments using a model made from a good thermal insulator (*e.g.* polystyrene or Rohacell where $k \approx 0.03\mathrm{W/mK}$) coated with wide-band crystal so that the measured surface temperature provides a good estimate of T_{ad} (see Newton *et al.,* 2009). Having estimated values of T_{ad} over the surface of the good insulator, a new model made from a poor insulator can then be used to determine h from transient experiments, as described above. By applying MLE to a three-temperature problem, both h and T_{ad} could be determined from a *single* transient experiment.

Numerical simulation showing how an MLE model can be used to determine h and T_{ad} from transient experiments is presented in Section 2. In Section 3, a novel IR sensor and the experimental apparatus used to validate the model are described, and experimentally-determined values of h and T_{ad} are compared with accepted

correlations in Section 4. The principal conclusions are presented in Section 5, and additional details of the MLE model are given in the Appendix.

2. Analysis of transient data

2.1 Analytical solutions of Fourier's equation

The nondimensional form of the 1D Fourier's equation (see Pountney *et al.* 2012) can be expressed as

$$\frac{\partial \Theta}{\partial Fo} = \frac{\partial^2 \Theta}{\partial Z^2} \tag{2.1}$$

where

$$\Theta = \frac{T - T_{in}}{T_{ad} - T_{in}} \tag{2.2a}$$

$$Fo = \frac{\alpha t}{L^2} \tag{2.2b}$$

and

$$Z = \frac{z}{L} \tag{2.2c}$$

T_{in}, z, L and α being the initial temperature of the solid, the normal distance from the heated surface, the thickness of the solid and its thermal diffusivity respectively.

For the case of a step-change in the fluid temperature, there are analytical solutions for two models that are particularly useful for experimenters: the *semi-infinite solid* and the *quenching problem*. The former model assumes that the slab has an infinite thickness and that the solution is valid for a slab of finite thickness L if the temperature change at $Z = 1$ is much smaller than the step-change in the fluid temperature; this limits the value of Fo for a transient experiment. In the quenching problem it is assumed that the back surface at $Z = 1$ is adiabatic; if the back surface could be perfectly insulated, the solution would be valid for any value of Fo.

The solution used here is for the quenching problem, the boundary conditions for which are:

$$-\left(\frac{\partial \Theta}{\partial Z}\right)_{z=0} = Bi(1 - \Theta_s) \tag{2.3a}$$

$$\left(\frac{\partial \Theta}{\partial Z}\right)_{z=1} = 0 \tag{2.3b}$$

The solution for the surface temperature, where $\Theta = \Theta_s$ at $Z = 0$, is given by

$$\begin{aligned} \Theta_s &= \frac{T_s - T_{in}}{T_{ad} - T_{in}} \\ &= 1 - 2\sum_{n=1}^{\infty} \exp(-\chi^2 \cot^2 \beta_n)\left(\frac{\sin \beta_n \cos \beta_n}{\beta_n + \sin \beta_n \cos \beta_n}\right) \end{aligned} \tag{2.4}$$

where

$$\chi = BiFo^{\frac{1}{2}} \tag{2.5a}$$

$$\beta_n = Bi \cot \beta_n \tag{2.5b}$$

and the Biot number is defined as

$$Bi = \frac{hL}{k_s} \tag{2.5c}$$

k_s being the thermal conductivity of the solid.

The effect of Bi on the variation of Θ_s with Fo computed from Eq. (2.4) by Pountney *et al.* (2012) is shown in Fig. 1. The 'semi-infinite solutions', and the loci of the 1% and 5% differences between the two solutions, are also shown; for $Bi < 16$ and $Fo < 0.2$, the differences are less than 1%. If a step-change could be achieved, and Fo were sufficiently small, either solution could be used. However, for slow transients where Fo is no longer small, the quenching problem provides a more useful analytical model.

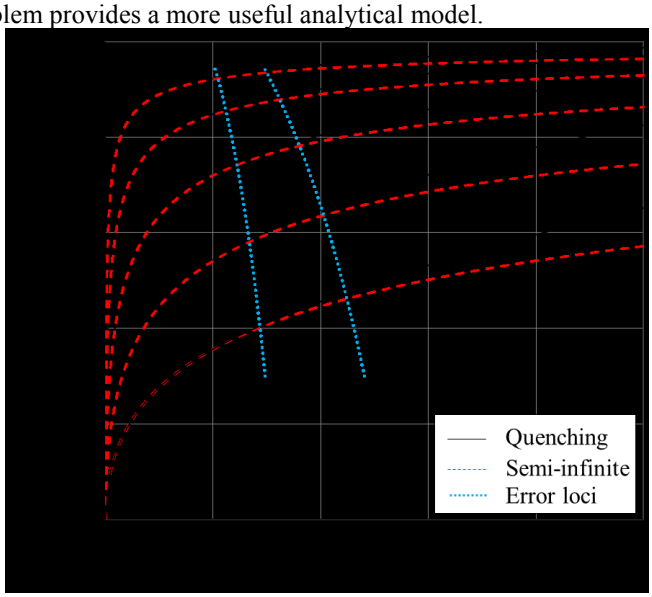

Fig. 1: Effect of Bi on variation of Θ_s with Fo for a step-change in fluid temperature (Pountney *et al.* 2012)

However, if a step-change cannot be generated at the test section, or if the back face of the test piece is not adiabatic, then the numerical method used below can be used.

2.2 Numerical solution of Fourier's equation

2.2.1 Numerical method

Details of the Maximum Likelihood Estimation (MLE) used below are given in the Appendix.

The Crank-Nicolson method was used for the numerical solutions of Fourier's equation, with step-lengths of $\delta Z = 0.01$ and $\delta Fo = 5.93 \times 10^{-6}$, and second-order derivatives were used for the convective boundary conditions at the two surfaces. The test piece (which corresponded to that used in the experiments described in Section 4) was 15-mm-thick polycarbonate, the properties of which were taken as $\rho = 1200\ \mathrm{kg/m^3}$, $k_s = 0.2\ \mathrm{W/mK}$ and $C_p = 1250\ \mathrm{J/kgK}$. A value of $Bi = 6.375$, corresponding to $h = 85\ \mathrm{W/m^2K}$ (which is typical of the experimental values) was used in the simulations; this is referred to as 'the true Biot number'.

For the simulations, given values of h and T_{ad} (which are referred to as the 'true values') were used in the *direct solution* of Fourier's equation to generate the time history of T_s for the quenching problem (*i.e.* an adiabatic back surface was assumed). The sampling rate of the simulated experimental data was 10 Hz, and normally-distributed random errors (modelling noisy measurements with a standard deviation of $\sigma = 0.2^{\circ}\mathrm{C}$) were added to the sampled values of T_s; the sampling rate and noise levels were representative of those used in the actual experiments. The noisy temperatures were then used as the boundary condition for the MLE model.

As T_{ad} was treated as an unknown for the MLE model, it is convenient to define three new nondimensional temperatures, all of which are based on $T_{s,max}$, the maximum value of the simulated surface temperatures. (As these temperatures were noisy, a smoothing curve was used to fit the data, and $T_{s,max}$ was taken as the maximum value of the smoothed data.) The new definitions are

$$\theta = \frac{T - T_{in}}{T_{s,max} - T_{in}} \qquad (2.6a)$$

$$\theta_s = \frac{T_s - T_{in}}{T_{s,max} - T_{in}} \qquad (2.6b)$$

and

$$\theta_{ad} = \frac{T_{ad} - T_{in}}{T_{s,max} - T_{in}} \qquad (2.6c)$$

The above definitions imply that $\theta_s = 1$ *and* $\theta_{ad} > 1$ when $T_s = T_{s,max}$. Fourier's equation, Eq. (2.1), and the boundary conditions, Eqs. (2.3a,b), are still valid if θ is replaced by θ.

For the simulations, it was assumed for the MLE that the adiabatic temperature could be represented by a two-term exponential series, where

$$\theta_{ad} = C_1\left(1 - \exp(-\frac{Fo}{Fo_{\tau_1}})\right) + C_2\left(1 - \exp(-\frac{Fo}{Fo_{\tau_2}})\right) \qquad (2.7)$$

where

$$Fo_\tau = \frac{\alpha\tau}{L^2} \qquad (2.8)$$

Consequently.

$$\left(\frac{Fo}{Fo_\tau}\right) = \frac{t}{\tau} \qquad (2.9)$$

and the steady-state value of θ_{ad} is equal to $C_1 + C_2$.

The four constants in Eq. (2.7), together with the values of Bi and σ, were computed by the MLE model. For the range of parameters used in this paper, a series of numerical experiments showed that accurate values of Bi could only be obtained if $N > 300$, where N is the number of values of T_s used in the computation, *and* if the duration of the experiment was large enough to ensure that the value of θ_{ad} was within 0.5% of its steady-state value. These limits are valid for the experimental results in Section 4 (where a 10 Hz sampling rate was used, $4 < Bi < 8$ and $Fo_\tau < 0.065$), but they should not be taken as a golden rule for all experiments. It is recommended that experimenters should become sufficiently familiar with the use of MLE to be confident in its application and limitation for their particular experiments.

2.2.2 Numerical simulations

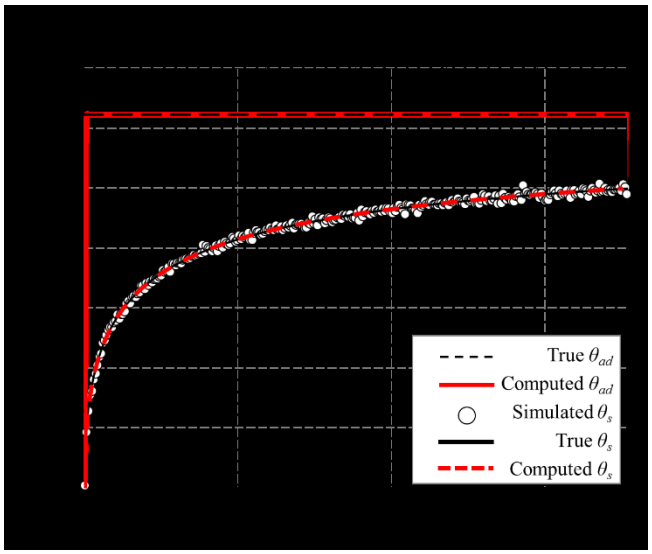

Fig. 2: Comparison between computed and true temperatures for perfect step-change in air temperature

Simulations are shown for three different transients in the air temperature: a perfect step-change; an approximate step-change; a slow transient. As stated above, $\theta_s = 1$ and $\theta_{ad} > 1$ when $T_s = T_{s,max}$.

Except for the perfect step change, a two-term exponential was used to generate the air temperature and, for all three different transient cases, a two-term exponential series (which was found to be necessary to represent the experimental results discussed in Section 4) was used for the MLE. The 'true values' of θ_s and θ_{ad} were used to generate the noisy data, as described above, and the computed values and 95% confidence interval of the computed Bi was found from the MLE model. Here, and in the cases discussed below, the value of the standard deviation in θ_s obtained from the MLE model agreed very closely with the value used to generate the noisy data.

Fig. 2 shows the case of a perfect step-change where the variations of the computed temperatures with Fo are in very good agreement with the true variations. The computed values of Bi and θ_{ad} were 6.381 ± 0.06 and 1.247, and these compared closely with the true values of 6.375 and 1.246 respectively. For this case, where the steady-state value of θ_{ad} was achieved at the start of the simulation, a value of $N = 3000$ was used for the computation.

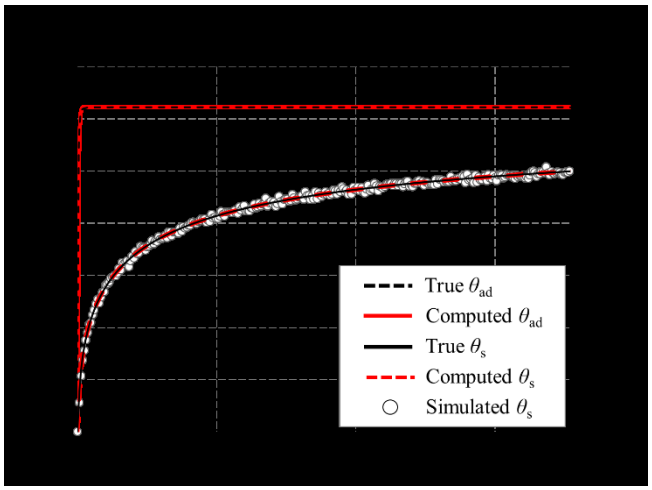

Fig. 3: Comparison between computed and true temperatures for approximate step-change in air temperature

Fig. 3 shows very good agreement for the case of the approximate step-change. The true value of θ_{ad} was produced with the values of C_1, C_2, Fo_{τ_1} and Fo_{τ_2} of $1.220, 0.025, 2.968 \times 10^{-4}$ and 0.05, respectively. As described above, a two-term exponential series (see Eq. (2.7)) was assumed for the MLE model, and the optimum values of C_1, C_2, $Fo_{\tau 1}$ and $Fo_{\tau 2}$ were computed to be $1.222, 0.0151, 2.968 \times 10^{-4}$ and 0.0423, respectively. The computed steady-state value of θ_{ad} was therefore found to be 1.237 compared with the true value of 1.245. The computed value of Bi was 6.515 ± 0.175, which compared with the true value of 6.375; the CI of $\pm$ 2.7 % captures the true value.

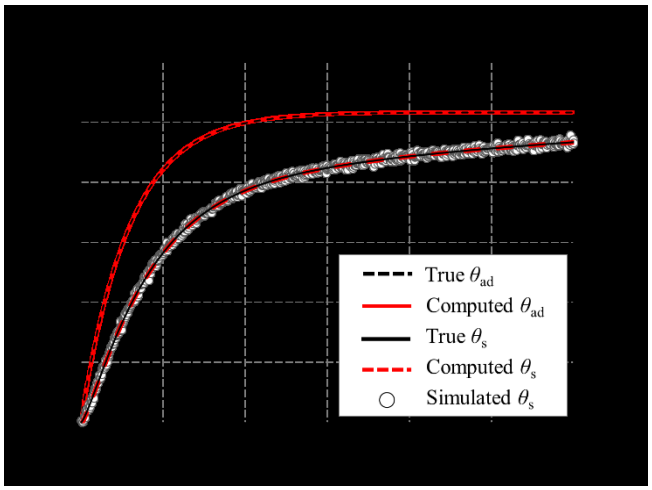

Fig. 4: Comparison between computed and true temperatures for slow transient in air temperature

Fig. 4 shows very good agreement for the case of a slow transient, where the values of $C_1, C_2, and\ Fo_{\tau_1} and\ Fo_{\tau_2}$ were $1.024, 0.01, 0.0593\ and\ 0.05$, respectively. The values of C_1, C_2, $Fo_{\tau 1}$ and $Fo_{\tau 2}$ produced by the MLE model were $1.023, 0.0194, 0.0593$ and 5.93×10^{-6} respectively, so that the computed steady-state value of θ_{ad} was 1.042 compared with the true value of 1.034. The computed value of Bi was 6.419 ± 0.094, which compares closely with the true value of 6.375; the CI of $\pm$ 1.5 % captures the true value.

In all the above simulations, the MLE model accurately captured the transient temperatures and the true value of the Biot number. The model is used in Section 4 to compute the values of Bi and θ_{ad} obtained from the experimental apparatus described in Section 3.

3. Experimental facility and IR temperature measurement

3.1 Experimental apparatus

Fig. 5 shows a close-up of the test section, which had a cross-section of 100 mm × 20 mm and a length of 400 mm. Air, with mainstream velocities up to $U_\infty = 40\ \mathrm{m/s}$, entered through a bell-mouth inlet and was extracted by a 'blower' (operating in the suction mode) downstream of the test section. An upstream 'mesh heater' (made to the design of Ireland *et al.* (1996) and powered by a 6 kW programmable supply (Magna-Power XR Series)) was used to generate an effective step-change of around 30 ℃ in the air temperature.

The test section was modular with 'target plates', or test pieces, constructed for different purposes, such as calibration of the IR sensor described below and for the experiments described in Section 4. Except for the IR calibration, the target plate was made from 15-mm-thick polycarbonate ($k = 0.2\ \mathrm{W/mK}$) and its surface was sprayed with black paint (Hallcrest SPBB). According to Kakade *et al.* (2009), the paint had an emissivity of 0.96, a thickness of approximately 10 μm, and (assuming a typical thermal conductivity of 0.2 W/mK) the temperature drop across the coating was estimated to be < 0.05 ℃. To minimise heat loss from the test section, the other surfaces were insulated with Rohacell 51 foam ($k_s = 0.03\ \mathrm{W/mK}$). The IR sensor was flush-mounted at the vertical-centre of the wall opposite the target plate and at a horizontal distance of 20 mm from it, and the sensor could be inserted at streamwise locations of $x = 80, 140$ and 200 mm, where x is the distance downstream from the mesh heater.

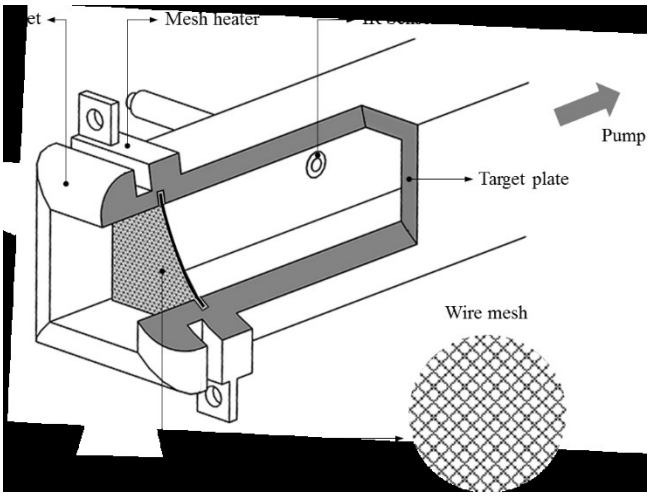

Fig. 5: Test section (Cho *et al.*, forthcoming)

3.2 Measurement of air velocity

The air velocity was measured using pitot tubes of 0.5-mm-diameter located in the air and static pressure taps in the wall of the test section at $x = 65, 125$ and 185 mm. The pressures were measured by a calibrated transducer (ESI PR3202), and the uncertainty in the velocity was estimated to be $\pm\ 0.7\ \mathrm{m/s}$.

The cross-sectional area of the wind tunnel, A, was 2000 mm^2 but, owing to the boundary layers on the four walls, the effective area, A_e, of the freestream outside the boundary layers decreased as x increased. As the experiments were conducted for incompressible flow, it follows from continuity that

$$U_\infty = \frac{U_0 A}{A_e} \qquad (3.1)$$

where U_0 is the freestream velocity at $x = 0$ and U_∞ is the value a distance x from the mesh. The value of A_e was calculated using a displacement thickness of $\delta^* \approx 0.125\ \delta$ for turbulent flow, where the boundary-layer thickness, δ, was taken as the value where $u/U_\infty = 0.99$, u being the streamwise velocity inside the layer. The values of U_∞ measured at $x = 65, 125$ and 185 mm were in good agreement with the values calculated from Eq. (3.1).

The wire mesh in the heater ensured that turbulent boundary-layer flow occurred from the start of the test section, and the velocity profiles were determined from cross-stream traverses of the pitot tubes at increments of 0.5 mm. As shown in Fig. 6a, the measured velocity profiles were consistent with the 1/7 power law (see White, 1994), where

$$\left(\frac{u}{U_\infty}\right)_{turb} = \left(\frac{y}{\delta}\right)^{1/7} \qquad (3.2)$$

Fig. 6b shows good agreement between the values of δ/x determined in this way and the correlation given by White (1994), where

$$\frac{\delta}{x} = 0.16 Re_x^{-\frac{1}{7}} \qquad (3.3a)$$

and

$$Re_x = \frac{\rho U_\infty x}{\mu} \qquad (3.3b)$$

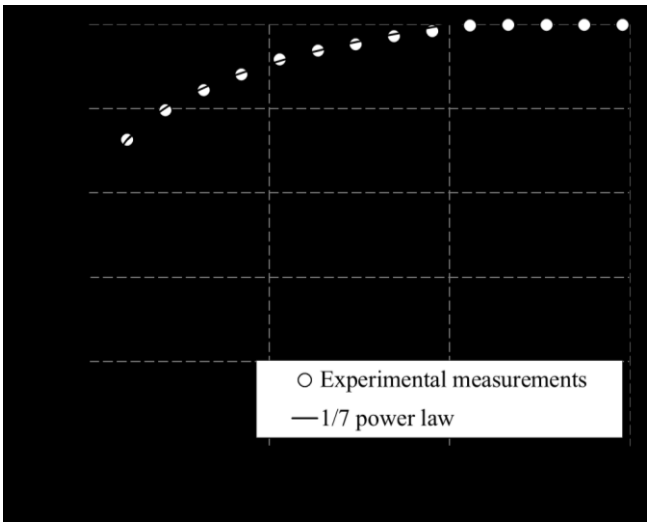

Fig. 6a: Typical velocity profile measured at $x = 185$ mm when $U_\infty = 30.6$ m/s and $\delta = 4.73$ mm (Eq. (3.2))

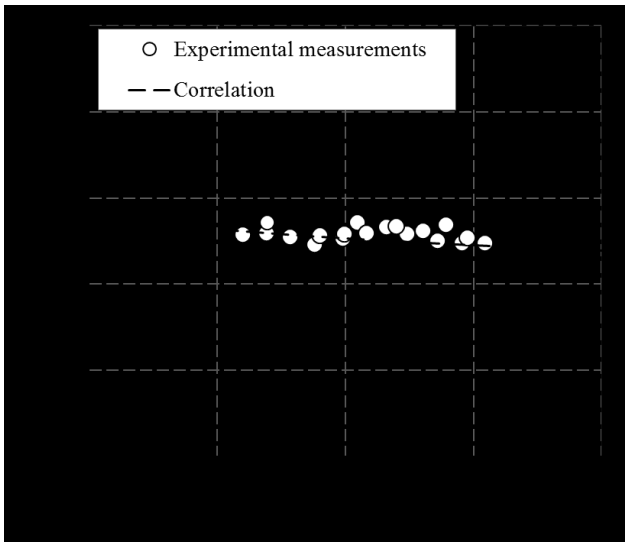

Fig. 6b: Comparison between measured boundary-layer thickness and correlation (Eq. (3.3a))

3.3 Measurement of air temperature

Fast-response thermocouples were manufactured using 0.025-mm-diameter K-type unsheathed wire with a beaded junction. The thermocouples, with a response time of 40 ms and a recovery factor of 0.72 (see Lock *et al.*, 2005) were used to measure the mainstream air temperature, T_∞, at $x = 25, 80, 140$ and 200 mm downstream of the mesh heater. The thermocouples were individually calibrated in a water bath, and the voltages were measured using a National Instrument USB-9213 input module and a pre-calibrated platinum-resistance thermometer; the

uncertainty in the temperature measurements was estimated to be ± 0.1 ℃. A typical step-change in air temperature measured at $x = 25$ mm using a fast response thermocouple is shown in Fig. 7.

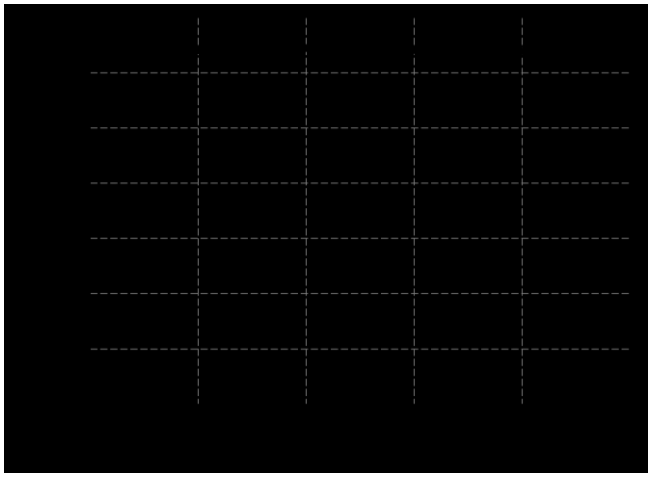

Fig. 7: Typical step-change in air temperature 25 mm downstream of mesh heater

3.4 Measurement of surface temperature

3.4.1 IR sensor

This section introduces a new IR sensing instrument which provided accurate temperature measurements under transient condition. The basic IR sensor used here (Melexis MLX90614ESF-DCI) was able to compensate for different levels of *steady* ambient temperature. However, it was unable to provide accurate measurements under *transient* conditions in its unconditioned state. A new instrument was designed to specifically address this problem and is described below.

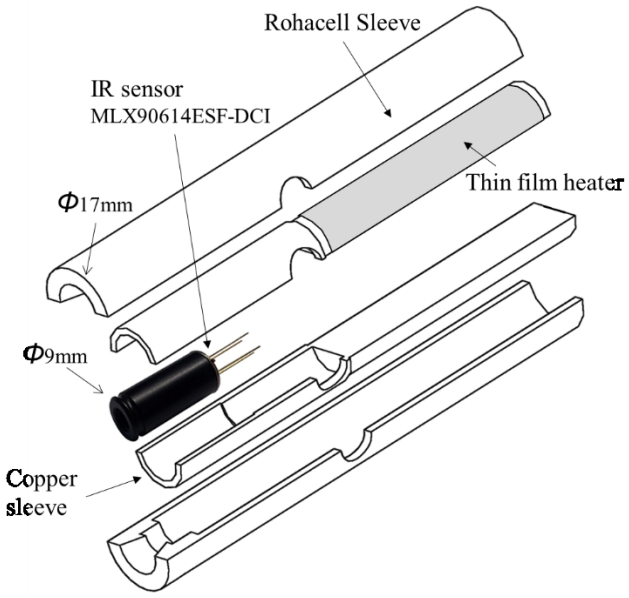

Fig. 8: Details of IR sensor (Cho *et al.*, forthcoming)

Figure 8 illustrates the IR sensor, which was an assembly of components developed by Cho (2014). The basic sensor, which had an outside diameter of 9 mm, was surrounded by a copper sleeve of 2 mm thickness, with 'thermal grease' used to reduce the contact resistance. A thin-film heater was used to heat the copper sleeve (and consequently the IR sensor), and the entire assembly was insulated by a 2-mm-thick sleeve of Rohacell 51 ($k = 0.03$ W/mK). The temperature of the basic IR sensor was measured by a built-in temperature sensor, and a PID (Proportional Integral Derivative) feedback controller was used to control the temperature to within ± 0.3 ℃ of its set value. When located 20 mm from the target plate, the sensor determined the average surface temperature over a circular area of approximately 6.7 mm diameter. The response time of the sensor was 0.1 s and the sample rate was up to 10 Hz.

3.4.2 Calibration of IR sensor

The calibration was first conducted under steady-state conditions and then under transient conditions to simulate the heat transfer experiments. For all calibrations (and subsequent tests) the sensor was set at a constant temperature of 35.0 ± 0.3 ℃, which was the typical average temperature in the transient experiments described in Section 4. Instead of the polycarbonate target plate used for the experiments, a 1-mm-thick copper plate was used for the calibration, and its surface was sprayed with the same black paint (Hallcrest SPBB) used on the target plates.

For the steady-state calibrations, the heated flow was left to stabilise, and the surface temperature was then simultaneously measured and averaged over a period of 30 s by both the IR sensor and a reference K-type thermocouple .The thermocouple, which was 0.025-mm-diameter and had a response time of 0.1s, was calibrated in a water bath; the estimated 95 % uncertainty was ± 0.1 ℃. For the transient calibrations, an approximate step-change in air temperature was created by the mesh heater, and the surface temperature of the copper plate was simultaneously measured by both the IR sensor and the reference thermocouple.

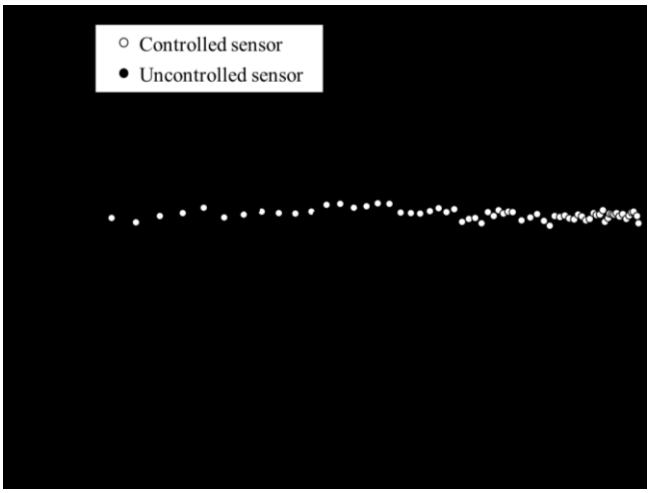

Fig. 9: Typical errors in transient tests for controlled and uncontrolled sensor

The errors shown in Fig. 9 were the differences between the IR measurements and T_{ref}, the latter being measured by the thermocouple in the copper plate; around 3000 data points were collected at 10 Hz as the surface was heated from 20 ℃ to 55 ℃. It can be seen that the transient measurements for the controlled sensor agree closely with the reference temperature whereas those for the uncontrolled sensor show a significant error that increases as the surface temperature increases. The controlled sensor was used for the experimental results discussed below, and the 95 % uncertainty in the surface temperature was estimated to be ± 0.2 ℃.

4. Transient heat transfer measurements

4.1 Analysis of experimental data

A series of transient heat transfer experiments was conducted at locations of $x = 80, 140$ and 200 mm. The measured surface temperatures were used, as described in Section 2, to compute both Bi and the transient values of θ_{ad}.

For the boundary conditions for Fourier's equation, the measured θ_s data were used for the front surface. As the temperature increase on the back surface was very small (less than 3 ℃ at $t = 300$ s), a laminar free-convection heat transfer coefficient was used as the boundary condition at $z = L$. The correlation given by Incropera *et al.* (2006) for an isothermal vertical surface is:

$$Nu = \frac{hl}{k_{air}} = \left(\frac{Gr}{4}\right)^{1/4} \frac{0.75Pr^{1/2}}{(0.609 + 1.221Pr^{1/2} + 1.238Pr)^{1/4}} \qquad (4.1)$$

where

$$Gr = \frac{g\beta(T_L - T_{amb})l^3}{\nu^2} \qquad (4.2)$$

Pr is the Prandtl number, Gr the Grashof number, g the gravitational acceleration, β the volume expansion coefficient, ν the kinematic viscosity, and $l = 50$ mm is the vertical height of the IR sensor measured from the bottom of the target plate. For the results discussed below, $0 < h_L < 2.2$ W/m^{2}K. In practice, the difference in

the solution of Fourier's equation using free-convection or adiabatic back surface boundary condition was quantitatively insignificant.

The front-surface temperatures were measured using the controlled IR sensor described in Section 3. The value of the experimental adiabatic-surface temperature was calculated from Eq. (1.2) using a recovery factor for turbulent flow over a flat plate of $R = Pr^{1/3}$, which for air corresponds to $R = 0.89$; T_∞ was determined from the fast response thermocouple, which had a recovery factor of 0.72; and U_∞ was measured by the pitot tube in the free stream. In the experiments, $T_{ad} - T_\infty$ was less than 0.7 ℃.

4.2 Experimental results

Two transient tests are discussed here: an approximate step-change ($Fo_\tau \approx 1.19 \times 10^{-4}$) and a slow transient ($Fo_\tau \approx 0.021$). The approximate step-change was achieved using the mesh heater described in Section 3, and the slow transient was obtained by gradually increasing the power output from the programmable supply.

Figure 10 shows a typical result for the approximate step-change case, where 3000 values of θ_s were collected over approximately 300 s. As described in Section 2, a two-term exponential series was assumed for θ_{ad} in the MLE model, and the computed results for θ_{ad} and θ_s show very good agreement with the measured values. The computed and measured maximum values of θ_{ad} were 1.269 ± 0.047 and 1.256, respectively; the measured value of $\theta_{ad,max}$ was taken as the maximum value of the smoothed data.

The computed Nusselt numbers were compared with the correlation given by Holman (1997) for turbulent boundary-flow over a flat plate where

$$Nu_x = \frac{hx}{k_{air}} = 0.0296 Re_x^{0.8} Pr^{\frac{1}{3}} \qquad (4.3)$$

For the experimental results, where $Re_x = 2.74 \times 10^5$, the value of Nu_x from Eq. (4.3) is 591; the computed value of 578.8 ± 16.6 is approximately 2 % lower than the correlation. The value of σ found from the MLE was 0.009, which corresponds to an uncertainty in the measured surface temperature of 0.2 ℃.

Figure 11 shows a typical result from a slow-transient test where again it can be seen that the agreement between the computed and measured values of θ_{ad} and θ_s is very good. The computed and measured values of $\theta_{ad,max}$ were 1.123 ± 0.016 and 1.130, respectively. For the experimental results, where $Re_x = 2.76 \times 10^5$, the value of Nu_x from Eq. (4.3) is 595; the computed value of 618.9 ± 43.2 is approximately 4% higher than the correlation. The value of σ found from the MLE was 0.014, which corresponds to an uncertainty in the measured surface temperature of 0.2 ℃.

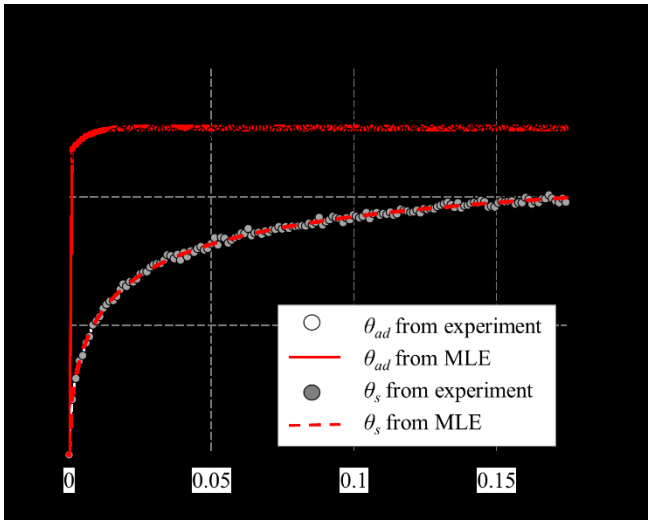

Fig. 10: Comparison between computed and measured temperatures for approximate step-change in air temperature ($Re_x = 2.74 \times 10^5$ and $x = 140$ mm)

Fig. 12 shows good agreement between the variation of Nu_x with Re_x determined from the experiments and the correlation calculated from Eq. (4.3). All data points shown in the figure were acquired from approximate step-change experiments, and $N = 3000$ was used for the analysis of each case. In most cases, the correlation was within the 95 % confidence intervals obtained from the MLE. (Five slow transient experiments were also conducted, and they all showed good agreement with the correlation.)

As air temperature data is not required by the MLE model to compute Nu_x and θ_{ad}, the model should also be applicable to the three-temperature problems discussed in Section 1.

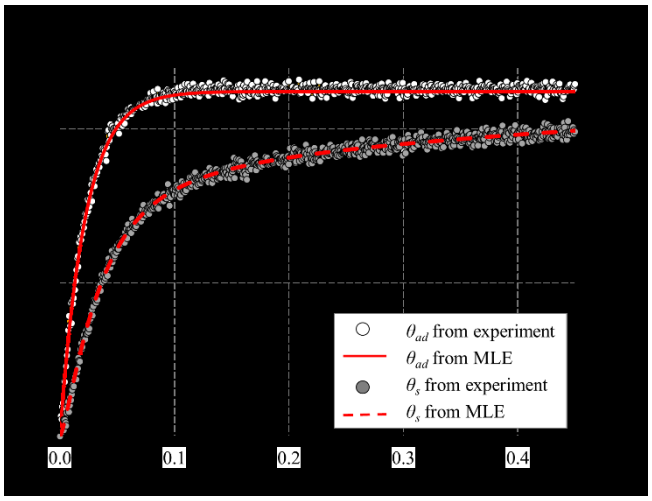

Fig. 11: Comparison between computed and measured temperatures for slow transient in air temperature ($Re_x = 2.76 \times 10^5$ and $x = 140$ mm)

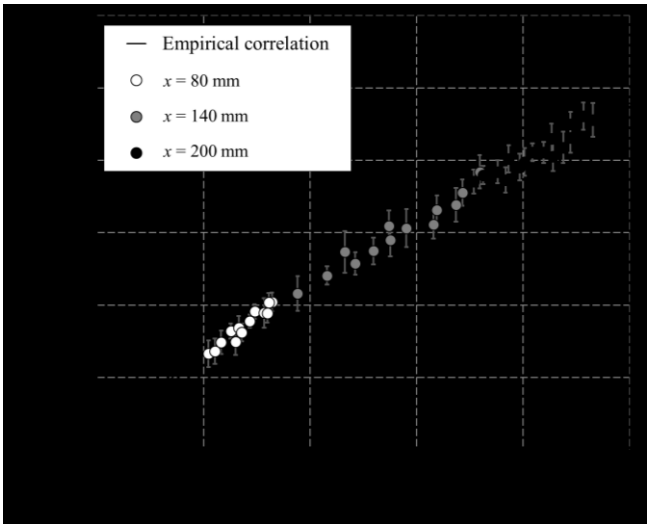

Fig. 12: Variation of Nu_x and CI with Re_x at three locations compared with empirical correlation (Eq. (4.3))

5. Conclusions

The big advantage of Maximum Likelihood Estimation, MLE, is that it can estimate the optimum values of h and T_{ad} , and their confidence intervals, from the numerical solution of the 1D Fourier's equation for any transient conditions. Importantly, this includes slow transients where the assumption of a semi-infinite-solid (which is assumed in most solutions) is invalid. If the boundary condition of the back face is known, or assumed, the numerical solution does not require the air temperature and needs only the surface-temperature history of the test piece.

Numerical simulations were used to demonstrate how MLE can be used to determine values of Bi and θ_{ad} (the nondimensional versions of h and T_{ad}) from transient surface-temperature measurements, and 'experimental' temperatures of a test piece were simulated by adding noise to the 'true' temperatures. The true temperatures were computed from the direct solution of Fourier's equation with specified values of Bi and θ_{ad}, and the back face of the test piece was assumed to be adiabatic. For the MLE, it was assumed that the transient variation of θ_{ad} could be represented by a two-term exponential series, with unknown amplitudes and time-constants, and Fourier's equation was used to compute values of Bi and θ_{ad} from the noisy data. For different thermal transients (including step-change and slow-transient cases), the computed values were shown to be in good agreement with the true values.

For the real experiments, a novel infra-red (IR) sensor, capable of measuring transient surface temperatures with an uncertainty of ± 0.2 ℃, was used in a purpose-built wind tunnel. A mesh heater was used to create a sudden

increase in the air temperature, T_∞, and the IR sensor was used to measure the transient surface temperatures on a flat wall of the wind tunnel. Transient values of T_∞ were measured with a fast-response thermocouple with an uncertainty of ± 0.1 ℃, and the steady air velocity was measured by a pitot tube with an uncertainty of ± 0.7 m/s. The boundary-layer flow over the wall was shown to be turbulent, and the transient values of T_{ad} were determined from the measured mainstream temperatures and velocities. For the boundary conditions for Fourier's equation, the measured surface temperatures were used for the front surface of the wall and a free-convection heat transfer coefficient was used for the back surface. Numerical solutions of Fourier's equation, obtained using MLE, gave values of the Nusselt numbers and adiabatic surface temperatures that were in good agreement with an empirical correlation for turbulent flow over a flat plate.

Suggestions were made about the length of time and number of data points needed to achieve accurate results, but it is recommended that experimenters should become sufficiently familiar with the use of MLE to be confident in its application to their particular experiments. The method applied here to boundary-layer flow with one stream of fluid could also be applied to 'three-temperature problems', like film cooling, which involve two streams of fluid. The advantage of using MLE for three-temperature problems is that *both* h and T_{ad} can be determined accurately from a *single* experiment.

References

Baughn, J. W. (1995). Liquid crystal methods for studying turbulent heat transfer. *Int. J. Heat Fluid Flow*, 16(5), 365-375. doi:10.1016/0142-727X(95)00042-O

Cho, G. (2014). *Hot gas ingress through turbine rim seals: heat transfer and fluid dynamics* (PhD Thesis, University of Bath, UK)

Cho, G. (forthcoming). Effect of ingress on turbine discs. *ASME J. Eng. Gas Turb. Power,* doi:10.1115/GT2015-42324

Davison, A. C. (2003). *Statistical models* (Vol. 11). Cambridge University Press. Cambridge

Gillespie, D. R. H., Wang, Z., Ireland, P. T., & Kohler, S. T. (1998). Full surface local heat transfer coefficient measurements in a model of an integrally cast impingement cooling geometry. *ASME J. Turbomach.*, 120(1). 92-99. doi:10.1115/1.2841394

Incropera, F. P., DeWitt, D. P., Bergmann, T. L., & Lavine, A. S. (2006). *Fundamentals of heat and mass transfer*, 6th ed. John Wiley & Sons, Hoboken.

Ireland, P.T., Gillespie, D.R.H., & Wang, Z. (1996). Heater element. *European patent*, (0847679)

Glezer, B., Owen, J. M., Pilbrow, R. G., & Syson, B. J. (1998). Application of Thermochromic Liquid Crystal to Rotating Surfaces. *ASME J Turbomach.,* 120(1), 100-103. doi:10.1115/1.2841369

Holman, J. P. (1997). *Heat transfer*, McGraw-Hill. New York.

Jones, T. V., & Hippensteele, S. A. (1988). High-resolution heat-transfer-coefficient maps applicable to compound-curve surfaces using liquid crystals in a transient wind tunnel. *NASA STI/Recon Technical Report N*, *89*, 10246

Kan, R., Guo, L., Ren, J., Huang, S., Jiang, H. D., & Yan, Y. Y. (2014). Determining mainstream reference temperature using the non-dimensional temperature analysis in the transient liquid crystal technique. *Int. J. Heat Mass Transfer*, 72, 201-209. doi:10.1016/j.ijheatmasstransfer.2014.01.018

Kasagi, N., Moffat R.J. and Hirata M. (1989). Liquid crystals. In: W.J. Yang, Editor, *Handbook of Flow Visualisation*, Hemisphere, New York

Lock, G. D., Yan, Y., Newton, P. J., Wilson, M., & Owen, J. M. (2005). Heat transfer measurements using liquid crystals in a preswirl rotating-disk system. *ASME J. Eng. Gas Turbines & Power,* 127(2), 375-382. doi:10.1115/1.1787509

Newton, P. J., Lock, G. D., Krishnababu, S. K., Hodson, H. P., Dawes, W. N., Hannis, J., & Whitney, C. (2009), Aero-thermal investigations of tip leakage flow in axial flow turbines: part 3- tip cooling*, ASME J. Turbomach.,* 131(1), pp 011008-1 - 011008-12., doi:10.1115/1.2950060

Newton, P. J., Yan, Y., Stevens, N. E., Evatt, S. T., Lock, G. D., & Owen, J. M. (2003). Transient heat transfer measurements using thermochromic liquid crystal. Part 1: An improved technique. *Int. J. Heat Fluid Flow*, 24(1), 14-22. doi:10.1016/j.ijheatmasstransfer.2014.01.018.

Pountney, O., Cho, G., Lock, G. D., & Owen, J. M. (2012). Solutions of Fourier's equation appropriate for experiments using thermochromic liquid crystal. *Int. J. Heat Mass Transfer*, 55(21), 5908-5915. doi:10.1016/j.ijheatmasstransfer.2012.06.001.

Pountney, O. J., Sangan, C. M., Lock, G. D., & Owen, J. M. (2013). Effect of Ingestion on Temperature of Turbine Disks. *ASME J Turbomach.,,* 135(5), 051010. doi:10.1016/S0142-727X(01)00125-4

Silvey, S. D. (1975). *Statistical inference,* Chapman and Hall, London.

Van Treuren, K. W., Wang, Z., Ireland, P. T., & Jones, T. V. (1994). Detailed measurements of local heat transfer coefficient and adiabatic wall temperature beneath an array of impinging jets. *ASME J Turbomach.,*, 116(3), 369-374. doi:10.1115/1.2929423

White, F. (1994). *Fluid mechanics, 3rd ed.* McGraw-Hill. New York

Yan, Y., & Owen, J. M. (2002). Uncertainties in transient heat transfer measurements with liquid crystal. *Int. J.Heat Fluid Flow*, 23(1), 29-35. doi:10.1016/S0142-727X(01)00125-4

Zhou, K., Wood, S. N., & Owen, J. M. (2013). Statistical and theoretical models of ingestion through turbine rim seals. *ASME J Turbomach.,* 135(2), 021014. doi: 10.1115/1.4006601

Appendix: Maximum Likelihood Estimation (MLE)

A1: Determination of empirical constants

MLE is a statistical method for estimating the value of empirical parameters from a given data set. Silvey (1975) and Davison (2003) give a detailed introduction to this method, and Zhou *et al.* (2013) used MLE to estimate the parameters, and their confidence intervals, in an orifice model for the prediction of ingress through turbine rim seals. In this paper, MLE is used to estimate values of Bi and θ_{ad} from measurements of the nondimensional surface temperatures θ_s.

First, a *likelihood function, P,* is developed: the *measured* nondimensional wall temperature, θ_s, is assumed to be normally distributed, with a standard deviation σ, around the *true* wall temperature, θ_w. The determination of θ_w depends on the two unknown parameters, Bi and θ_{ad}, so that $\theta_s \sim \mathcal{N}(\theta_w(Bi, \theta_{ad}), \sigma^2)$, where $\mathcal{N}$ denotes a normal distribution and $\theta_w(Bi, T_{ad})$ denotes that θ_w is a function of Bi and θ_{ad}. The likelihood function can therefore be expressed as

$$P = \frac{1}{(2\pi\sigma^2)^{\frac{N}{2}}} \exp\left(-\sum_{i=1}^{N} \frac{\left(\theta_{s,i} - \theta_{w,i}(Bi, \theta_{ad})\right)^2}{2\sigma^2}\right) \qquad \text{(A.1)}$$

where N is the number of data points.

Instead of maximising P to find the most likely values of σ, Bi and θ_{ad}, it is more convenient to minimize l, the negative logarithm of P, where

$$l = \frac{N}{2}\ln(2\pi) + N\ln(\sigma) + \frac{1}{2\sigma^2}\sum_{i=1}^{N}\left(\theta_{s,i} - \theta_{w,i}\right)^2 \qquad \text{(A.2)}$$

The minimisation is achieved using Newton's method.

As Bi depends mainly on the fluid dynamics, it is assumed to be constant in the transient heat transfer experiments. For a slow transient, where the air temperature changes with time, θ_{ad} is time-dependent, and it is assumed that it tends to its steady-state value in an exponential manner. For the experiments discussed in this paper, a two-term exponential series was found to give acceptable results, hence,

$$\theta_{ad} = C_1\left(1 - \exp\left(-\frac{Fo}{Fo_{\tau_1}}\right)\right) + C_2\left(1 - \exp\left(-\frac{Fo}{Fo_{\tau_2}}\right)\right) \qquad \text{(A.3)}$$

MLE is then used to determine the four constants $C_1, C_2, Fo_{\tau_1}, Fo_{\tau_2}$ together with the values of Bi and σ.

A2: Calculation of confidence intervals

Let $\boldsymbol{\phi}$ denote a generic parameter vector (for example, $[\sigma, Bi, C_1, Fo_{\tau_1}, C_2, Fo_{\tau_2}]$), and let $\boldsymbol{\phi_o}$ denote the parameter vector estimated from MLE. From Davison (2003), it can be shown that, for large N,

$$\boldsymbol{\phi} \sim \mathcal{N}(\boldsymbol{\phi_o}, (\partial^2 l)/(\partial\boldsymbol{\phi}\partial\boldsymbol{\phi}^T)^{-1}) \qquad \text{(A.4)}$$

$(\partial^2 l)/(\partial\boldsymbol{\phi}\partial\boldsymbol{\phi}^T)^{-1}$, which is the covariance matrix of the parameters, can be used to construct the confidence intervals for components of $\boldsymbol{\phi_o}$. Let σ_k denote the k^{th} square root of the leading diagonal element of the matrix, then the corresponding 95 % confidence interval is $\phi_{o,k} \pm 1.96\,\sigma_k$.

(The MLE for this paper was coded in MATLAB language, and the negative likelihood function, l, was minimized using the 'lsqnonlin' function to obtain the parameters as well as its hessian matrix, $\partial^2 l/(\partial\boldsymbol{\phi}\partial\boldsymbol{\phi}^T)$. The inverse of the hessian matrix was used to calculate the confidence intervals.)